Available online at www.sciencedirect.com

ScienceDirect

Geochimica et Cosmochimica Acta 267 (2019) 240–256

Geochimica et Cosmochimica Acta

www.elsevier.com/locate/gca

Re-examining thermal metamorphism of the Renazzo-like (CR) carbonaceous chondrites: Insights from pristine Miller Range 090657 and shock-heated Graves Nunataks 06100

Jemma Davidson [a,b,*], Devin L. Schrader [b], Conel M.O'D. Alexander [a], Larry R. Nittler [a], Roxane Bowden [c]

[a] Department of Terrestrial Magnetism, Carnegie Institution of Washington, 5241 Broad Branch Road, Washington DC 20015-1305, USA
[b] Center for Meteorite Studies, School of Earth and Space Exploration, Arizona State University, 781 East Terrace Road, Tempe, AZ 85287-6004, USA
[c] Geophysical Laboratory, Carnegie Institution of Washington, 5251 Broad Branch Road, Washington DC 20015-1305, USA

Received 12 March 2019; accepted in revised form 18 September 2019; available online 26 September 2019

Abstract

We re-examine the Renazzo-like (CR) chondrite metamorphic trend based on Cr_2O_3 contents of FeO-rich olivine, indicating that it is only appropriate to use such analyses to identify the endmembers of this group (i.e., those that have experienced either no detectable heating or significant heating). As such Miller Range (MIL) 090657 appears to have experienced very minimal (if any) thermal processing and is one of the most pristine CR chondrites analyzed to date, while Graves Nunataks 06100 is the most shock-heated CR chondrite studied.

On the basis of bulk H-C-N isotopic compositions, MIL 090657 appears to be of petrological type 2.7. We also report the H-C-N isotopic compositions of extracted insoluble organic matter, *in situ* chemical compositional data, presolar grain abundances, and a petrologic description of MIL 090657. As a minimally altered CR chondrite of relatively high mass (133.1 g), MIL 090657 provides an invaluable opportunity to perform coordinated, often destructive, analyses on pristine CR chondrite material.

By combining a number of petrographic characteristics (Cr_2O_3-content of ferroan olivine, Co/Ni ratios of Fe,Ni metal, ratios of Fe# in chondrule olivine and low-Ca pyroxene, and the presence of excess silica in chondrule plagioclase) with bulk isotopic compositions, we demonstrate their utility as indicators for determining the relative pristinity/heating of low petrographic (type 1–3) chondrites.

Keywords: CR chondrites; Pristine meteorites; Primitive meteorites; Presolar grains; MIL 090657; GRA 06100

1. INTRODUCTION

After chondritic porous interplanetary dust particles, some members of the Renazzo-like (CR) carbonaceous chondrites represent some of the most pristine (i.e., least altered since accretion) extraterrestrial samples available for study (e.g., Weisberg et al., 1993; Abreu and Brearley, 2010; Schrader et al., 2015). The least altered of the CR chondrites contain abundant presolar grains (e.g., Floss and Stadermann, 2009a,b; Davidson et al., 2014a), organic matter (e.g., Alexander et al., 2007; Martins et al., 2007; Floss et al., 2014; Le Guillou and Brearley, 2014), and Fe-rich amorphous silicates (e.g., Abreu and Brearley,

* Corresponding author at: Center for Meteorite Studies, School of Earth and Space Exploration, Arizona State University, 781 East Terrace Road, Tempe, AZ 85287-6004, USA.
E-mail address: jdavidson@asu.edu (J. Davidson).

https://doi.org/10.1016/j.gca.2019.09.033
0016-7037/

2010; Howard et al., 2015a) that can provide valuable insights into early Solar System conditions and the first stages of parent body processing. The CR chondrites cover the whole range of aqueous alteration, from ~CR3 (least altered) to CR1 (most altered), and have been extensively studied by a wide variety of analytical techniques (e.g., Schrader et al., 2008, 2011, 2015; Alexander et al., 2013; McBride et al., 2013; Davidson et al., 2014a; Floss et al., 2014; Howard et al., 2015a). These chondrites are also scientifically important as their chondrules share similarities with comet Wild 2 particles (e.g., Nakashima et al., 2012; Defouilloy et al., 2017; Schrader et al., 2018a), and the CR chondrite parent body may have formed in the outer Solar System beyond the orbit of Jupiter (Warren, 2011) and perhaps even Saturn (Van Kooten et al., 2016). Therefore, minimally altered CR chondrites may provide us with a record of outer Solar System material for comparison with inner Solar System material (e.g., Warren, 2011), such as the least altered unequilibrated ordinary chondrites like Semarkona (LL3.00).

Queen Alexandra Range (QUE) 99177 and Meteorite Hills (MET) 00426 are two of the best-studied CR chondrites due to their minimally altered nature (e.g., Abreu and Brearley, 2010). Unfortunately, their total known weights are relatively small at 31.3 g (MET 00426) and 43.6 g (QUE 99177), respectively (Satterwhite and Mittlefehldt, 2001), effectively limiting the opportunities for conducting destructive analyses. Due to their scientifically valuable nature, sample requests for both non-destructive and destructive analyses have resulted in a sharp decrease in CR chondrites available for study (McBride et al., 2013). Therefore, identifying new minimally altered samples is extremely important.

An isotopic study of the CR chondrites showed that the bulk O-isotope composition of CR2 Miller Range (MIL) 090657 is similar to that of MET 00426, suggesting that it is minimally aqueously altered (Schrader et al., 2014). MIL 090657 has a low weathering grade of Be, remnant fusion crust, a fracturing grade of A, and a relatively large total mass of 133.1 g (Satterwhite and Righter, 2012). Thus, MIL 090657 provides an invaluable opportunity to perform coordinated, often destructive, analyses on minimally altered CR chondrite material. We report the H-C-N isotopic compositions of bulk material and extracted insoluble organic matter (IOM), *in situ* chemical compositional data, presolar grain abundances, and a petrologic description of MIL 090657.

While most CR chondrites have experienced only low-temperature aqueous alteration (at least <88 °C; Jilly-Rehak et al., 2018), a number are recognized to be more thermally processed via impact heating, including Graves Nunataks (GRA) 06100 and Grosvenor Mountains (GRO) 03116 (e.g., Abreu and Bullock, 2013; Alexander et al., 2013; Schrader et al., 2015). Grossman and Brearley (2005) showed that it is possible to investigate the degree of thermal metamorphism experienced by the least heated (petrologic types 3.0–3.2) unequilibrated ordinary chondrites (UOCs) and Ornans-like carbonaceous chondrites (COs) on the basis of the Cr_2O_3 contents of FeO-rich olivine. In minimally altered samples, Cr is uniformly distributed in ferroan chondrule olivine, but exsolves into lamellae and then diffuses toward grain peripheries with increasing degree of thermal metamorphism (Grossman and Brearley, 2005). Therefore, by determining the mean and standard deviation of Cr_2O_3 contents of olivine grain cores we can determine a sample's relative degree of heating within individual chondrite groups. In order to do that, we must first understand how such compositional trends behave within specific, individual chondrite groups. The UOC trend is well-established, the CO trend was recently revised (Davidson et al., 2014b, 2019), and the CM chondrite trend was recently defined (Schrader and Davidson, 2017); we aim to do the same here for the CR chondrites. A potential trend was tentatively defined for the CR chondrites by Schrader et al. (2015), but an error in their analytical method yielded erroneous results, which is discussed below.

In this study, we aim to: (1) re-examine the relative degree of heating experienced by CR chondrites on the basis of Cr_2O_3 contents of FeO-rich olivine, (2) investigate the degree of heating experienced by MIL 090657 compared to MET 00426 and QUE 99177, and (3) compare MIL 090657 with the thermally altered end member GRA 06100 within the CR chondrite group.

2. ANALYTICAL PROCEDURE

2.1. Mineralogy and petrology analyses

A polished thin section of MIL 090657,6 was initially characterized with an optical microscope (Electronic Annex-1; EA-1). Full section, high-resolution backscattered electron (BSE) images and X-ray element maps of individual chondrules were then obtained on C coated thin sections (operating conditions: 15.0 kV and ~1 nA) with the JEOL JSM-6500F field emission scanning electron microscope (FE-SEM) at the Carnegie Institution of Washington (CIW). These maps show the elemental and mineralogical distributions within the sample, and were used to identify mineral phases for study, including FeO-rich olivine (both chondrules and chondrule fragments). Apparent chondrule diameters were determined by measuring the major and minor axes of chondrules in BSE images using Adobe Photoshop®.

Major and minor element abundances of silicate mineral phases were analyzed (Mg, Si, Na, Ti, Mn, Al, Fe, Ni, Cr, and Ca; 15 kV accelerating voltage, 30 nA probe current) with a JEOL 8900 electron probe microanalyzer (EPMA) at CIW. Metal and sulfide phases were analyzed (Fe, S, Ni, Co, Cu, Cr, Al, P, Si; 15 kV, 20 nA) with a JEOL 8900 EPMA at the Smithsonian Institution and a Cameca SX-100 at the University of Arizona. The analyses were conducted with a 1 μm beam, a Phi-Rho-Z correction method, and counting times of 30 seconds on the peak and 15 seconds on each background for a total of 60 seconds per element (with the exception of Cr, Al, Mn, and Ti for silicate and magnetite analyses, and P, Co, Si, Cu, and Cr for metal and sulfide mineral analyses when counting times of 60 s on the peak and 30 s on each background for a total of 120 s per element was used).

Only stoichiometric olivine, pyroxene, plagioclase, metal and sulfide analyses with totals between 98.0–102 wt.% were retained and are presented here (Tables 1–3). Detection limits (in wt.%) and standards used are listed in Table 2 for silicate analyses and Table 3 for metal and sulfide analyses. Data are provided in EA-2.

For comparison with the chondrule silicate data accumulated from MIL 090657, we also performed quantitative analyses on silicate phases from the shock-heated CR2 chondrite GRA 06100 (e.g., Abreu and Bullock, 2013; Alexander et al., 2013; Schrader et al., 2015). We utilized literature data from thin section GRA 06100,26 (Schrader et al., 2015) and obtained additional analyses on the same thin section with the Cameca SX-100 at the University of Arizona using the same operating conditions described above for MIL 090657,6.

2.2. Bulk meteorite and organic matter isotopic analyses

A 1 g chip of MIL 090657 bulk sample was acquired and crushed to a grain size of <150 μm. Aliquots were analyzed for the bulk H (2.3 and 1.8 mg), C and N (8.3 mg) after the method of Alexander et al. (2012). An IOM residue was subsequently prepared using the CsF–HF technique described in Alexander et al. (2010), which, through leaching/washing with 2 N HCl, milliQ water, dioxane, and an immiscible mixture of CsF–HF solution (1.6–1.7 g/cc) and dioxane, effectively removed non-IOM phases including most soluble organic compounds known to be present in chondrites. Aliquots of IOM (typically 0.2–0.4 mg) were then analyzed for H, C and N after the method of Alexander et al. (2010).

Elemental and isotopic analyses were made with a Thermo Finnigan Delta^{plus}XL mass spectrometer at CIW. Sample gases were introduced into the mass spectrometer via a molecular sieve gas chromatographic column connected to: (1) a Carlo Erba NA 2500 series elemental analyzer for C and N analyses, or (2) a Thermo Finnigan thermal conversion elemental analyzer for H analyses where a He-flushed autosampler was used to reduce the amount of atmospheric water adsorbed. In order to monitor the accuracy of the measured isotopic ratios and elemental compositions, internal working gas standards and external standards were analyzed at regular intervals for all analyses. See Alexander et al. (2010, 2012) for more analytical details.

2.3. NanoSIMS ion imaging

Matrix areas (~12,000 μm^2 total) within the MIL 090657,6 thin section were subjected to raster ion imaging via high-resolution (nanoscale) secondary ion mass spectrometry (Cameca NanoSIMS 50L at CIW) using automated mapping routines. Matrix areas were presputtered with a focused Cs^+ primary ion beam and currents of ~100–130 pA for typically 7 minutes until sputter equilibrium was reached. A ~ 1.7 pA Cs^+ primary ion beam was used to image 10 × 10 μm^2 (256 × 256 pixel) areas, yielding a spatial resolution of ~150 nm. In order to locate O- and C-anomalous presolar grains and C-anomalous carbonaceous material, secondary electrons and $^{16,17,18}O^-$, $^{12}C_2^-$, $^{12}C^{13}C^-$, $^{28}Si^-$, $^{27}Al^{16}O^-$ were analyzed simultaneously (10 frames per "image" with a ~34 min analysis time). A mass resolution of m/Δm = 9000 (Cameca definition) was used to resolve interferences from neighboring peaks (e.g., ^{17}O from ^{16}OH). The isotopes $^{28}Si^-$ and $^{27}Al^{16}O^-$ were measured to distinguish between silicate and oxide grains.

Ion image data were processed and quantitatively analyzed with the L'IMAGE software (L. R. Nittler, CIW). Prior to the identification of isotopically anomalous regions, images were corrected for deadtime (44 ns), stage and/or beam drift between frames, and for quasi-simultaneous arrival effects; see Nittler et al. (2018) for more detail on typical measurement conditions and complete data reduction procedures.

Table 1
CR chondrites, in approximate order of least to most thermally altered, according to FeO-rich olivine Cr2O3 composition.

Meteorite	Sample Number	σ-Cr_2O_3	Mean Cr2O3 (wt.%)	# Analyses	Source
MIL 090657	,6	0.092	0.393	39	a
EET 96259	,12	0.095	0.418	14	b
QUE 99177	,6	0.100	0.348	38	b
Shisr 033	UA2159,1	0.100	0.422	30	b
Gao-Guenie (b)	UA2301,1	0.102	0.374	74	b
PCA 91082	,15	0.104	0.390	27	b
Al Rais	USNM1794-8	0.114	0.378	18	b
GRA 95229	,22	0.119	0.400	22	b
GRO 03116	,15	0.119	0.373	32	b
LAP 04720	,8	0.122	0.371	53	b
MET 00426	,33	0.126	0.404	5*	b
LAP 02342	,14	0.143	0.386	35	b
EET 87770	,31	0.144	0.365	41	b
Y-793495	,72–2	0.145	0.330	23	b
NWA 801	UA2300,1	0.152	0.386	57	b
GRA 06100	,26	0.189	0.328	25	b

Sources: (a) this study; (b) values recalculated in this study from data in Schrader et al. (2015). Published data for MET 00426 (Berlin, 2009) and QUE 99177 (Abreu and Brearley, 2010) are not included here as specific values were not provided in the source references. *Indicates too few analyses to be considered statistically significant.

Table 2
Representative silicate analyses in ferromagnesian chondrules and matrix olivine in MIL 090657,6.

	Chondrules																Matrix	
Chondrule[a]	Ch1	Ch2	Ch3	Ch5	Ch7	Ch8	Ch10	Ch11	Ch5	Ch3	Ch7	Ch8	Ch1	Ch4	Ch5	Ch6	G1	G2
Chondrule Type[b]	I	II	I	I	I	I	II	II/AO	I	I	I	I	I	I	I	I	II	II
Silicate Type[c]	Ol	Ol	Ol	Ol	Ol	Ol	Ol	Ol	LCP	LCP	LCP	LCP	HCP	Plag	Plag	Plag	Ol	Ol
Chemical composition (wt.%)																		
SiO_2	41.42	36.88	41.41	41.70	41.78	40.12	35.44	41.41	58.11	58.48	58.16	57.28	46.28	52.03	44.25	49.53	39.68	34.18
TiO_2	0.06	bdl	bdl	bdl	bdl	bdl	bdl	bdl	0.10	0.13	0.11	0.15	1.20	0.50	bdl	0.56	bdl	bdl
Al_2O_3	0.30	0.02	0.03	0.03	0.02	0.04	bdl	0.08	0.72	0.93	0.65	1.18	11.02	24.58	33.31	26.36	0.02	0.42
Cr_2O_3	0.13	0.51	0.64	0.45	0.56	0.78	0.29	0.65	0.73	0.89	0.68	1.09	1.43	0.38	bdl	0.53	0.32	0.18
FeO	0.51	24.44	2.69	1.41	1.81	4.77	33.15	3.50	1.14	1.85	1.24	2.79	1.90	1.05	1.56	1.06	13.46	44.16
MnO	bdl	0.47	0.29	0.10	0.15	0.59	0.52	0.13	0.28	0.15	0.16	0.39	0.34	0.26	bdl	0.64	0.20	0.62
MgO	55.60	36.77	53.82	55.72	55.32	51.61	29.01	54.38	37.58	37.81	38.11	36.08	15.53	6.57	0.94	3.60	46.82	19.50
CaO	0.46	0.18	0.18	0.24	0.19	0.25	0.32	0.17	0.71	0.39	0.52	0.57	20.82	13.60	18.94	16.50	0.11	0.55
Na_2O	bdl	bdl	bdl	bdl	bdl	bdl	bdl	bdl	bdl	bdl	bdl	bdl	0.07	1.20	0.09	1.02	bdl	0.25
NiO	bdl	bdl	bdl	bdl	bdl	0.07	bdl	bdl	bdl	bdl	bdl	bdl	0.14	bdl	0.07	bdl	0.07	bdl
Total	98.48	99.27	99.06	99.65	99.83	98.23	98.73	100.32	99.37	100.63	99.63	99.53	98.73	100.17	99.16	99.80	100.68	99.86
Cation formula based on 4 oxygens for olivine, 6 for pyroxene, and 8 for plagioclase																		
Si	0.990	0.982	0.995	0.989	0.991	0.985	0.991	0.986	1.976	1.968	1.972	1.961	1.703	2.371	2.076	2.296	0.985	1.000
Ti	0.001	bdl	bdl	bdl	bdl	bdl	bdl	bdl	0.003	0.003	0.003	0.004	0.033	0.017	bdl	0.020	bdl	bdl
Al	0.008	0.001	0.001	0.001	0.001	0.001	0.000	0.002	0.029	0.037	0.026	0.048	0.478	1.322	1.842	1.440	0.001	0.014
Cr	0.002	0.011	0.012	0.008	0.011	0.015	0.006	0.012	0.020	0.024	0.018	0.030	0.042	0.014	bdl	0.019	0.006	0.004
Fe	0.010	0.544	0.054	0.028	0.036	0.098	0.776	0.070	0.032	0.052	0.035	0.080	0.058	0.040	0.061	0.041	0.279	1.081
Mn	bdl	0.011	0.006	0.002	0.003	0.012	0.012	0.003	0.008	0.004	0.005	0.011	0.011	0.010	bdl	0.025	0.004	0.015
Mg	1.980	1.459	1.927	1.971	1.957	1.888	1.210	1.930	1.905	1.897	1.926	1.842	0.852	0.447	0.066	0.249	1.732	0.851
Ca	0.012	0.005	0.005	0.006	0.005	0.007	0.010	0.004	0.026	0.014	0.019	0.021	0.821	0.665	0.952	0.819	0.003	0.017
Na	bdl	bdl	bdl	bdl	bdl	bdl	bdl	bdl	bdl	bdl	bdl	bdl	0.005	0.106	0.008	0.091	bdl	0.014
Ni	bdl	bdl	bdl	bdl	bdl	0.001	bdl	bdl	bdl	bdl	bdl	bdl	0.004	bdl	0.003	bdl	0.001	bdl
Total	3.004	3.012	2.999	3.006	3.003	3.007	3.005	3.007	3.998	3.999	4.003	3.996	4.007	4.991	5.008	5.000	3.012	2.997
Fe#	1	27	3	1	2	5	39	3	2	3	2	4	6				14	56
Fa	1	27	3	1	2	5	39	3									14	56
Fo	99	73	97	99	98	95	61	97									86	44
En									97	97	97	95	49					
Fs									2	3	2	4	3					
Wo									1	1	1	1	47					
An														86	99	90		
Ab														14	1	10		
Fe/Mn	–	51	9	14	12	8	63	27	4	12	8	7	6				66	70

bdl = below detection limit.

Standards used for silicate analyses (with detection limits in wt.%) were forsterite for Mg (0.02) and Si (0.03), cossyrite for Na (0.03) and Ti (0.03), spessartine for Mn (0.03) and Al (0.01), fayalite for Fe (0.04), Ni-olivine for Ni (0.05), chromite for Cr (0.03), and diopside for Ca (0.02).

[a] Ch = chondrule, G = single mineral grain in matrix.

[b] I = type I FeO-poor chondrule, II = type II FeO-rich chondrule, AO = agglomeratic olivine chondrule.

[c] Ol = olivine, LCP = low-Ca pyroxene, HCP = high-Ca pyroxene, and Plag = plagioclase.

Table 3
Representative major and minor element compositions of opaque minerals (wt.%) in MIL 090657,6 chondrules.

Location[a]	Ch1	Ch1	Ch2	Ch2	Ch2	Ch6	Ch7	Ch10	Ch10	Ch11	Ch11	Ch11	Ch11
Grain[b]	OA1	OA2	OA1	OA1	OA2	OA1	OA2	OA1	OA1	OA1	OA4	OA5	OA5
Ch. Type[c]	I	I	II	II	II	I	I	II	II	II/AO	II/AO	II/AO	II/AO
Op. Type[d]	met	met	po	pn	pn	met	met	Ni-met	po	po	met	Ni-met	Ni-po
Si	bdl	bdl	bdl	bdl	bdl	bdl	bdl	0.02	bdl	0.02	0.02	0.03	0.03
P	0.35	0.55	bdl	bdl	bdl	0.26	0.27	0.12	bdl	bdl	0.33	bdl	bdl
S	bdl	bdl	36.9	34.4	33.8	bdl	bdl	0.03	36.3	36.4	bdl	bdl	34.7
Cr	0.26	0.40	0.07	bdl	0.03	0.11	0.28	bdl	0.10	0.06	0.35	0.07	0.11
Fe	94.3	93.0	62.1	40.9	38.4	95.0	89.0	79.3	62.8	62.3	92.7	71.5	50.5
Co	0.20	0.26	bdl	0.38	0.41	0.23	0.39	0.96	0.15	0.25	0.37	1.11	0.14
Ni	3.97	5.18	1.17	23.9	26.1	4.34	9.71	18.5	0.29	0.60	5.25	25.8	13.6
Cu	nd	nd	bdl	0.34	0.18	nd	nd	bdl	bdl	bdl	bdl	bdl	bdl
Al	nd	nd	bdl	bdl	bdl	nd	nd	bdl	bdl	bdl	0.03	0.03	bdl
Total	99.1	99.4	100.3	100.0	99.0	99.9	99.6	98.9	99.6	99.7	99.0	98.6	99.0

bdl = below detection limits.
Standards used for metal and sulfide analyses (with detection limits in wt.%) were Si-metal for Si (0.02), indium phosphide for P (0.03), chalcopyrite for S (0.02), Fe (0.13) and Cu (0.12), chromite for Cr (0.02), Co-metal for Co (0.13), Ni-metal for Ni (0.10), and anorthite for Al (0.02).
Mn (0.06). Ti (0.02), Mg (0.03), and Ca (0.02) were also analyzed but were below their detection limits (shown in parentheses) and are not included here.
[a] Ch = chondrule.
[b] OA = opaque assemblage.
[c] I = type I chondrule, II = type II chondrule, and II/AO = hybrid type II/agglomeratic olivine chondrule.
[d] met = Ni-poor metal, Ni-met = Ni-rich metal, Ni-po = Ni-rich pyrrhotite, po = pyrrhotite, pn = pentlandite.

3. RESULTS

3.1. Chromium content of ferroan olivine in CR chondrites

Analyses performed on 39 distinct grain cores of FeO-rich chondrule olivine grains in MIL 090657,6 yielded a mean Cr_2O_3 content of 0.39 wt.% with a one standard deviation σ-Cr_2O_3 of 0.09 (Fig. 1; Table 1). The Cr_2O_3 averages and standard deviations for other CR chondrites (Table 1), including GRA 06100, were collated, or calculated, from published data (Abreu and Brearley, 2010; Berlin, 2009; Schrader et al., 2015); this is discussed further in Section 4.1.

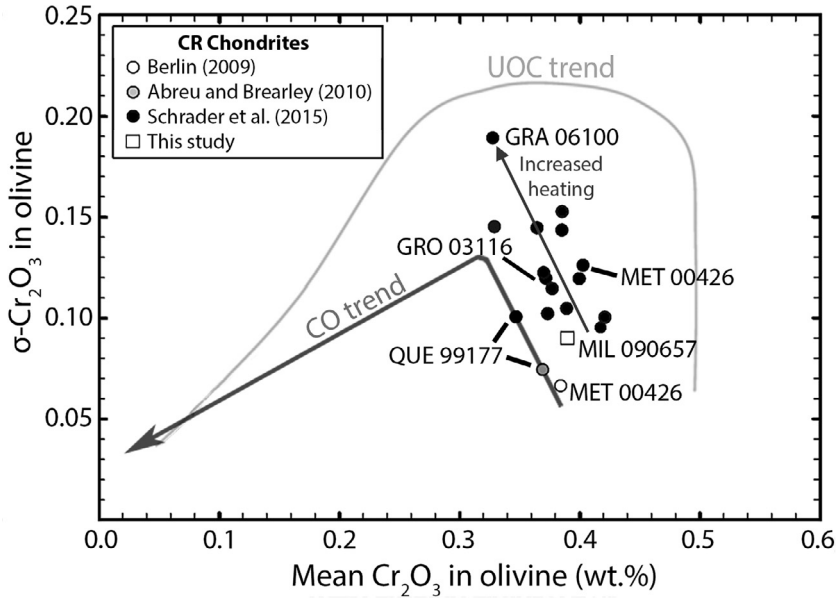

Fig. 1. Plot of the standard deviation (σ) versus the mean of the Cr_2O_3 content (in weight percent) of ferroan olivine in MIL 090657, GRA 06100, GRO 03116 and other CR chondrites. Trends for the unequilibrated ordinary chondrites (UOC; Grossman and Brearley, 2005) and Ornans-like carbonaceous chondrites (CO3; Davidson et al., 2014b) are shown for comparison. Additional data from: Berlin (2009), Abreu and Brearley (2010), and Schrader et al. (2015). Data from Schrader et al. (2015) have been recalculated from data presented in an electron annex. Published data for MET 00426 (Berlin, 2009) and QUE 99177 (Abreu and Brearley, 2010) were determined from Fig. 17 in Abreu and Brearley (2010) as values were not provided.

3.2. MIL 090657: Isotopic compositions of bulk meteorite and extracted organic matter

MIL 090657 has a bulk isotopic and elemental composition of $\delta^{13}C = -2.1‰$ (1.25 wt.% C), $\delta^{15}N = 183‰$ (0.078 wt.% N), and $\delta D = 814‰$ (0.314 wt.% H), yielding a bulk C/H (wt.) ratio of 3.98. Fig. 2 shows how the bulk C/H ratios and bulk δD values vary amongst the CR chondrites; using these criteria, MIL 090657 appears to be the least altered CR chondrite and contrasts significantly with shock-heated GRA 06100.

Insoluble organic matter extracted from MIL 090657 has an isotopic composition of $\delta^{13}C = -18.5‰$ (61.8 wt.% C), $\delta^{15}N = 131.9‰$ (2.22 wt.% N), and $\delta D = 2716‰$ (4.36 wt.% H). MIL 090657 IOM has a H/C ratio of 0.847 (at.), which is the highest of all CRs measured to date (Alexander et al., 2017). Figure EA-3 shows the C- and N-isotopic compositions of IOM from MIL 090657 compared to IOM from other CR chondrites and other carbonaceous chondrite groups. However, the yield of IOM isolated from MIL 090657 was also the lowest for any CR (Alexander et al., 2007, 2010), accounting for only 0.236 wt.% C in the bulk meteorite. It is not clear if this low yield was an analytical artifact or a reflection of the nature of the organic C in this meteorite.

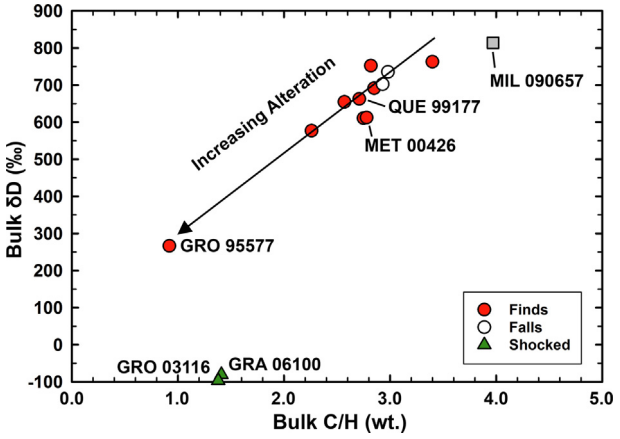

Fig. 2. The H isotopic composition (δD in per mil) versus C/H ratio (by weight) of bulk MIL 090657 (this study; gray square) and other CR chondrites, including the heated and shocked GRA 06100 and GRO 03116 (Alexander et al., 2012, 2013). A general trend of alteration is shown.

3.3. MIL 090657: Mineralogy and petrology

3.3.1. General description and modal mineralogy

The MIL 090657,6 thin section contains abundant large chondrules, chondrule fragments, and mineral grains in an optically dark matrix (EA-1). The thin section consists of ~94 vol.% silicate and ~6 vol.% opaque minerals (not including rust). Opaque minerals are present in both chondrules and interchondrule matrix. Apparent chondrule diameters range from 0.1 mm to 4.0 mm; despite this variability, the mean diameter of 0.63 ± 0.12 mm (±2SE; n = 100 chondrules) is similar to the 0.70 mm average previously reported for the CR chondrites (e.g., Weisberg et al., 1993, 2006; Schrader et al., 2015).

3.3.2. Chondrule textural types and silicate mineralogy

The dominant chondrule textural types are porphyritic-olivine-pyroxene and porphyritic-olivine chondrules. A small number of barred olivine chondrules and one rare agglomeratic olivine (AO) chondrule were also identified. The chondrule population, which is typical for a CR chondrite (e.g., Weisberg et al., 1993; Jones, 2012; Schrader et al., 2015; Tenner et al., 2015), is dominated by FeO-poor (type I: Fe/[Fe + Mg] < 10% atomic ratio) chondrules (>95 vol.%), with fewer FeO-rich (type II: Fe/[Fe + Mg] > 10% atomic ratio) chondrules (~4 vol.%), and a rare Al-rich chondrule (<1 vol.%).

We obtained 87 compositional analyses of silicate minerals in six type I chondrules (see representative analyses in Table 2). FeO-poor type I chondrules are predominantly forsteritic; olivine has a compositional range of $Fa_{0.5–4.9}$, with Fe/Mn (molar) of 3–50 (31 analyses). Low-Ca pyroxene (LCP; Wo < 5) ranges from $Fs_{1.6–7.2}$ and $Wo_{0.5–4.4}$ (41 analyses), while high-Ca pyroxene (HCP; Wo > 5) ranges from $Wo_{5.4–48.6}$ (15 analyses). The mean Fe# (where Fe# = Fe/[Fe + Mg] * 100) values calculated from multiple analyses of olivine and low-Ca pyroxene within individual chondrules are within one Fe# of one another (Table 4). The ratios of the Fe# of olivine and low-Ca pyroxene for individual chondrules show little variability; they are all 1 within 1σ error (range: 0.7 ± 0.4 to 1.1 ± 0.3; Table 4).

Table 4
Iron number (Fe#) for olivine (ol) and low-Ca pyroxene (px) (averages with 1σ errors) of individual FeO-poor (type I) chondrules in MIL 090657,6 and GRA 0610026.

Meteorite	Chondrule	Fe# ol	Fe# px	Fe# ol/Fe# px (1σ)	Source
MIL 090657,6	Ch3	2.9 (0.9)	2.6 (0.2)	1.1 (0.3)	a
MIL 090657,6	Ch4	2.1 (0.1)	2.6 (0.7)	0.8 (0.3)	a
MIL 090657,6	Ch5	1.3 (0.4)	2.0 (0.3)	0.7 (0.4)	a
MIL 090657,6	Ch7	1.6 (0.3)	2.4 (0.8)	0.7 (0.4)	a
MIL 090657,6	Ch8	3.0 (1.5)	3.3 (0.5)	0.9 (0.5)	a
GRA 06100,26	Ch10	3.2 (0.8)	2.1 (0.1)	1.5 (0.2)	b
GRA 06100,26	Ch11	1.8 (1.0)	1.4 (0.2)	1.3 (0.6)	a
GRA 06100,26	Ch12	5.4 (0.6)	3.9 (0.7)	1.4 (0.2)	a
GRA 06100,26	Ch13	2.5 (0.3)	2.3 (0.3)	1.1 (0.2)	a

Sources: (a) this study; (b) data from this study combined with data from Schrader et al. (2015).

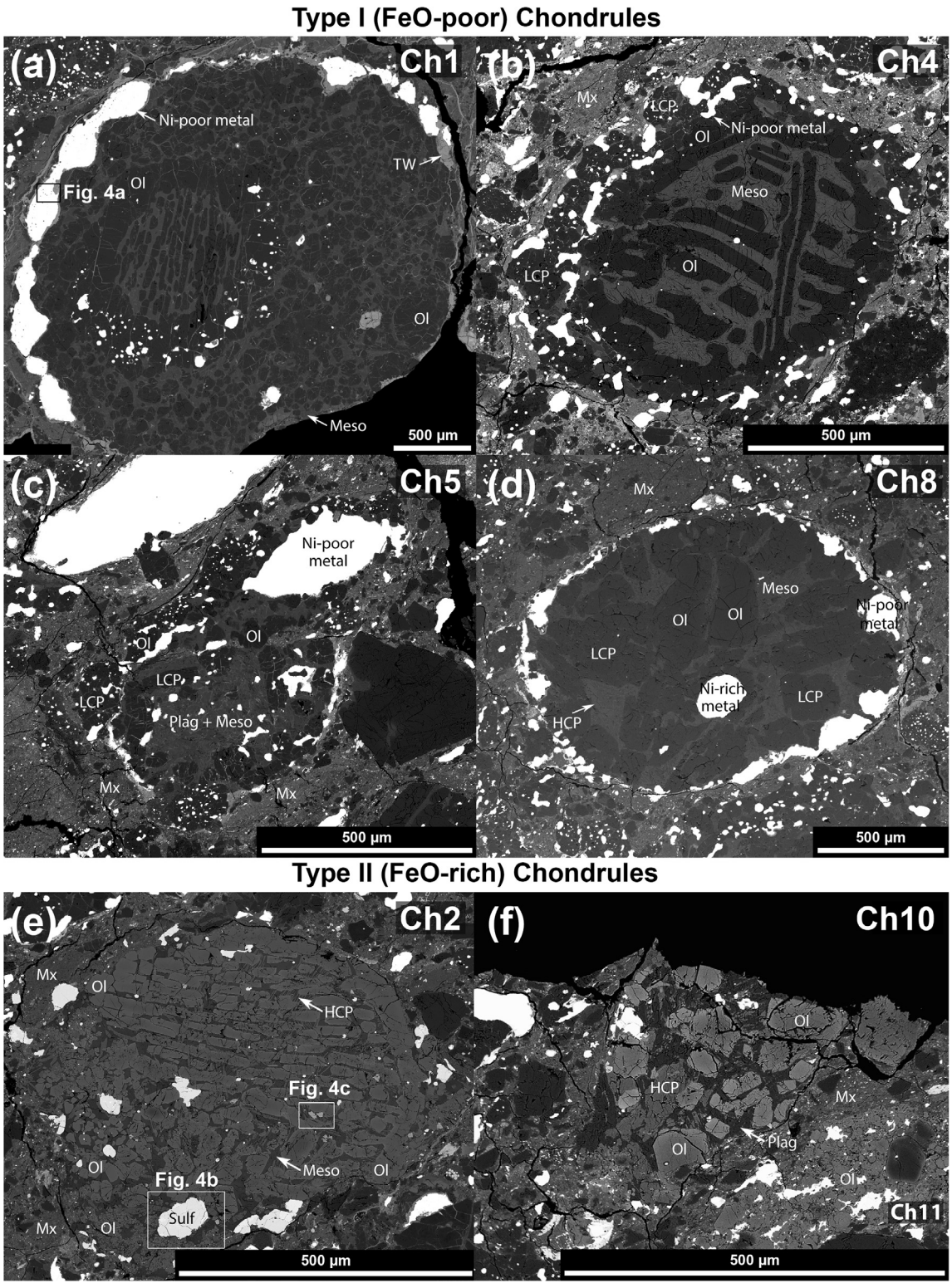

Fig. 3. BSE images of representative (a–d) FeO-poor type I, and (e, f) FeO-rich type II chondrules in MIL 090657,6. (a) Large porphyritic, multi-generational chondrule (Ch1), with opaque phases mostly at the exterior of both the inner enveloped chondrule and outer enveloping chondrule, (b) FeO-poor barred olivine chondrule (Ch4), (c) possible Al-rich chondrule (ARC) with abundant plagioclase, mesostasis, and Ni-poor metal (Ch5), (d) porphyritic FeO-poor chondrule (Ch8), (e) sulfide-bearing, FeO-rich barred olivine chondrule (Ch2), (f) FeO-rich porphyritic chondrule (Ch10) and adjacent FeO-rich agglomeratic olivine chondrule (Ch11). Where HCP = high-Ca pyroxene, LCP = low-Ca pyroxene, Meso = mesostasis, Mx = matrix, Ol = olivine, Plag = plagioclase, Sulf = sulfide, and TW = terrestrial weathering. Higher magnification images of marked opaque phases are shown in Fig. 4. See EA1 for the location of chondrules within the thin section.

We obtained a further 130 compositional analyses of silicate minerals in 3 type II chondrules and 37 type II chondrule fragments and mineral grains ($Fa_{3.5–56.0}$; 88 analyses) (e.g., Table 2). FeO-rich type II chondrules are compositionally variable (~$Fa_{13.9}$ to Fa_{56}; 86 analyses), normally zoned (e.g., ~Fa_{27} to Fa_{34} in Ch2; core to rim), and contain FeO-poor relict grains (e.g., $Fa_{3.5–5.0}$; 2 analyses; Fig. 3f). Isolated FeO-rich olivine grains in the matrix are compositionally similar to type II chondrules (Table 2), and are considered to be chondrule fragments (as previously noted by Schrader et al., 2013, 2015; Frank et al., 2014). Relict FeO-poor olivine within one type II/AO chondrule (Chondrule 11) has a compositional range of $Fa_{3.5–5.0}$, with Fe/Mn molar ratios of 26 to 27 (2 analyses; Table 2). FeO-rich olivine ranges from $Fa_{13.9–56.0}$, with Fe/Mn of 27 to 132 (86 analyses). The Cr_2O_3 abundances of FeO-rich olivine grain cores range between 0.18–0.63 wt. %, for an average of 0.39 wt.% and a standard deviation of 0.09 wt.% (39 analyses; Fig. 1). Compositions of LCP range from $Fs_{5.5–10.8}$ and $Wo_{1.9–3.7}$ (4 analyses), while HCP compositions ranges from $Wo_{16.8–46.2}$ (3 analyses).

3.3.3. Plagioclase compositions

Plagioclase phenocrysts were analyzed in six chondrules (five FeO-poor type I, one FeO-rich type II) from MIL 090657 and had compositions of $An_{76–99}$. The excess silica molar fraction, $[\ ]Si_4O_8$, within chondrule plagioclase was calculated per the method of Beaty and Albee (1980) using the following formulae:

$$Ca(Fe,Mg)Si_3O_8 = 4 - (Si + Al) \quad (1)$$

$$[\ ]Si_4O_8 = 1 - [Na + Mg + K + Ca + Fe + Ba - Ca(Fe,Mg)Si_3O_8] \quad (2)$$

Calculated excess silica abundances range from –0.48 mol.% to 9.6 mol.%; the plagioclase in the five chondrules (four FeO-poor, one FeO-rich) all show resolvable silica excesses.

3.3.4. Chondrule opaque assemblages

Opaque assemblages (OAs) are located predominantly along the exteriors, but also within the interiors, of some chondrules (Fig. 3). OAs consist of abundant metal (primarily kamacite, with minor taenite), less abundant sulfides (pyrrhotite and pentlandite), and minor chromite (Fig. 4).

The opaque mineralogies of the type I chondrules studied here consist entirely of Fe,Ni metal typically, but not exclusively, located at the chondrule peripheries. The Fe, Ni-metal is Ni-poor, and compositions range in Ni from 4.0 wt.% to 9.7 wt.%, and Co from 0.15 wt.% to 0.43 wt. % (28 analyses; Table 3, Fig. 5). The Fe,Ni metal grains often contain micron sized sub-grains of silica, chromite, and Fe- and Cr-sulfide (Fig. 4a).

The opaque mineralogies of type II chondrules are more complex, containing chromite, Ni-rich metal, rare Ni-poor metal, pyrrhotite, and pentlandite (e.g., Fig. 4b). The composition of Ni-rich metal ranges from 15.1 wt.% to 25.8 wt.% Ni, and 0.93 wt.% to 1.2 wt.% Co (9 analyses; Table 3, Fig. 5), while rare Ni-poor metal has 5.2 wt.% to 5.3 wt.% Ni, and 0.37 wt.% to 0.42 wt.% Co (2 analyses; Table 3,

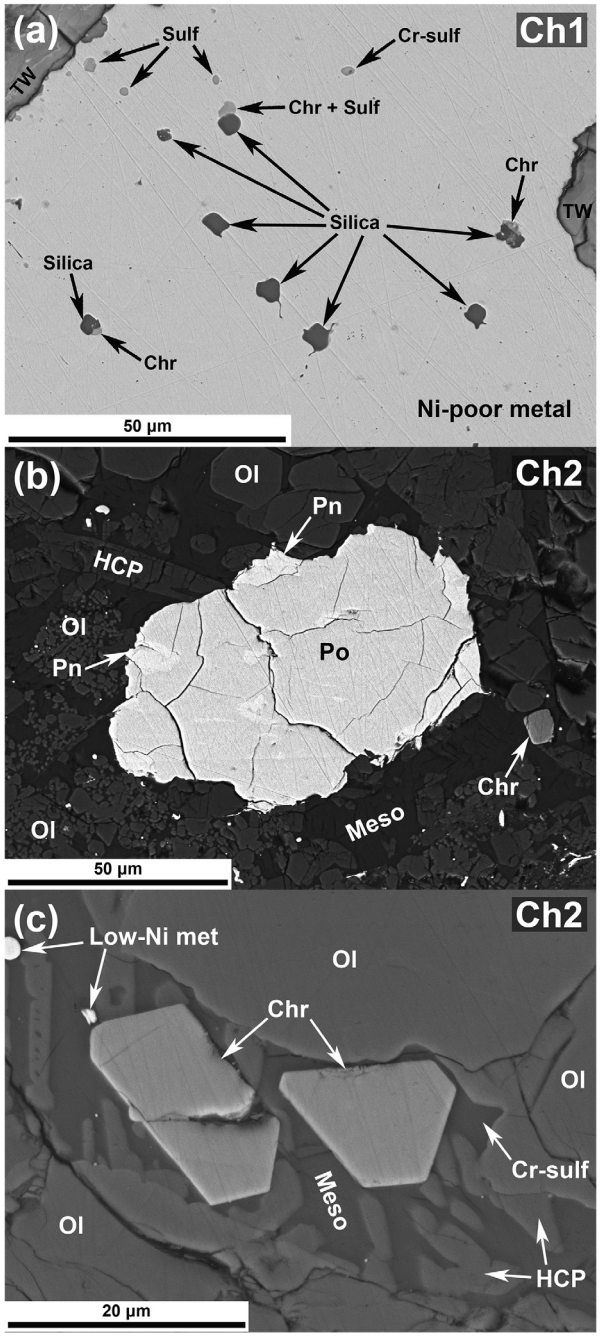

Fig. 4. BSE images of representative opaque assemblages in (a) FeO-poor type I and (b, c) FeO-rich type II chondrules. (a) A portion of a large Ni-poor metal grain at the exterior of Chondrule 1 containing isolated inclusions of silica, chromite (Chr), and Cr-bearing sulfides (Cr-sulf), the exterior of which has experienced some terrestrial weathering (TW). (b) An Fe-sulfide assemblage in Chondrule 2 composed primarily of pyrrhotite (Po) with minor pentlandite (Pn) and a nearby subhedral chromite grain surrounded by mesostasis and FeO-rich olivine (both porphyritic and micro-porphyritic). (c) Euhedral chromite grains in the pyroxene-bearing mesostasis of FeO-rich Chondrule 2. Where; Chr = chromite, Cr-sulf = Cr-bearing sulfide, HCP = high-Ca pyroxene, Low-Ni met = low-Ni metal, Meso = mesostasis, Ol = olivine, Pn = pentlandite, Po = pyrrhotite, and TW = terrestrial weathering. See Fig. 3 for locations of opaque minerals within chondrules.

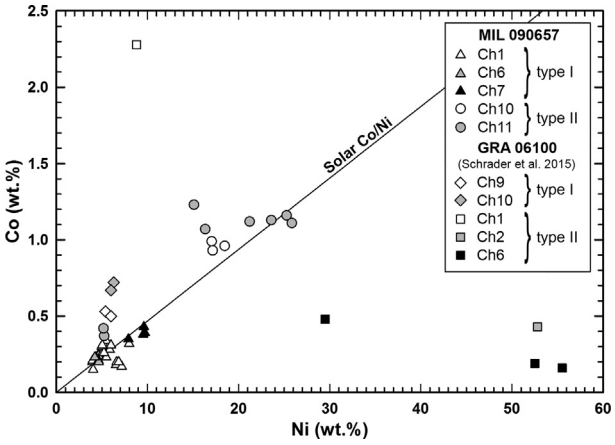

Fig. 5. Cobalt and Ni (both weight percent) content of individual metal grains in chondrules from MIL 090657,6 and GRA 06100,26. Metal grains from MIL 090657 exhibit a positive correlation between Ni and Co, indicating that this sample has experienced minimal heating. In contrast, GRA 06100 data, from Schrader et al. (2015), show that Ni-rich metal is depleted in Co relative to Ni-poor metal, similar to observations of metal in the thermally metamorphosed CO and ordinary chondrites (Kimura et al., 2008), and Vigarano-like carbonaceous (CV) chondrite RBT 04133 (Davidson et al., 2014c). The solar Co/Ni ratio line is shown for reference (data from Lodders et al., 2009).

Fig. 5). Chromite grains are euhedral to subhedral (Fig. 4c). The Ni-rich metal is associated with the sulfides pyrrhotite and pentlandite, which often occur as pyrrhotite-pentlandite intergrowths (Fig. 4b). Pyrrhotite contains minor amounts of Ni (0.17–1.2 wt.%), Co (0.15–0.25 wt.%), Cr (0.5–0.10 wt.%), and Cu is entirely below the detection limit (bdl) of 0.12 wt.% (7 analyses; Table 3). The Fe/S (at.) ratios range from 0.97 to 1.00, indicating that, despite these grains containing minor elements, pyrrhotite is the pyrrhotite group sulfide troilite (FeS). One Ni-rich pyrrhotite analysis (potentially overlapping with pentlandite), contains 13.6 wt.% Ni, 0.14 wt.% Co, 0.11 wt.% Cr, and no detectable Cu. Pentlandite displays a range of Ni contents (23.9–26.4 wt.%), as well as minor Co (0.31–0.47 wt.%), Cr (bdl–0.04 wt.%; detection limit = 0.02 wt.% Cr), and Cu (0.18–0.34 wt.%) (7 analyses; Table 3).

No magnetite was seen within chondrules, though very small, rare magnetite framboid clusters are present in the matrix; individual magnetite framboids are <1 μm in diameter, the largest framboid cluster observed is ~7 × 12 μm.

3.4. MIL 090657: Presolar grains

NanoSIMS ion image mapping of matrix identified numerous presolar grains (silicate, oxide, and SiC), and three isotopically anomalous carbonaceous regions that are most likely organic matter. In total, 27 presolar O-anomalous (silicate + oxide) grains were identified, corresponding to an abundance in the matrix of ~112 ± 25 ppm. This abundance error is based solely on counting statistics (Gehrels, 1986) and is thus likely an underestimate since it does not account for uncertainties in determining grain sizes from ion images. Comparison with the Monte Carlo modeling of Nittler et al. (2018) suggests that the true uncertainty may be on order of 40% larger. Moreover, this abundance estimate is based on a relatively small analysis area (~12,000 μm^2). Six presolar SiC grains were also identified, giving a matrix abundance of 40 ± 20 ppm. Three carbonaceous regions with resolvable anomalous C isotopic compositions at the three sigma level have $\delta^{13}C$ values of up to ~ 100‰, similar to those seen in MET 00426 and QUE 99177 (e.g., Floss et al. 2014; Le Guillou and Brearley, 2014).

3.5. GRA 06100

We used literature data from Schrader et al. (2015) (7 olivine and 2 LCP analyses) and obtained 53 additional analyses of olivine (30 analyses) and LCP (23 analyses) from four type I chondrules. The FeO-poor olivine has a compositional range of $Fa_{1.2–7.0}$, with Fe/Mn molar ratio of 3 to 32 (37 analyses), while LCP ranges from $Fs_{1.3–4.7}$ and $Wo_{0.5–4.4}$ (25 analyses). The average Fe# values of olivine and low-Ca pyroxene for two of the four individual chondrules differ in Fe# within 1σ error (Table 4). The ratios of the Fe# of olivine to the Fe# of low-Ca pyroxene range from 1.1 ± 0.2 to 1.5 ± 0.2 (errors are 1σ) for individual chondrules.

4. DISCUSSION

4.1. Defining a metamorphic sequence: Cr_2O_3-content of ferroan olivine

For the least altered unequilibrated ordinary and CO chondrites, it is possible to identify the most minimally thermally metamorphosed samples by determining the Cr_2O_3-content of ferroan olivine following the procedures of Grossman and Brearley (2005). This scheme has been calibrated for the unequilibrated ordinary chondrites (UOCs) (Grossman and Brearley, 2005), CO chondrites (Grossman and Brearley, 2005; Davidson et al., 2014b, 2019), the CM chondrites (Schrader and Davidson, 2017), and tentatively for the CR chondrites (Davidson et al., 2015a; Schrader et al., 2015). Since the initial Cr composition of ferroan olivine may differ between chondrite groups, it is not appropriate to directly compare between groups. Rather this scheme should be used to internally compare within chondrite groups. Following the procedures of Grossman and Brearley (2005), we analyzed the Cr_2O_3 contents of the centers of 39 different ferroan olivine grains within type II chondrules and chondrule fragments in MIL 090657,6.

The data from Schrader et al. (2015) were recalculated here (Table 1); this was necessary because, by including data obtained from grain rims and including multiple data points from individual chondrules, the study did not accurately follow the procedure of Grossman and Brearley (2005). This led to a bias in each sample by weighting the mean and σ to chondrules with more data, as well as increasing mean Cr_2O_3 contents by incorrectly including analyses of typically Cr-rich grain rims. As a result, it was not possible to use this technique to identify any

shock-heated CR chondrites, which is addressed here (Fig. 1 and Table 1); with the data set correctly analyzed, the most shock-heated CR chondrite GRA 06100 (Abreu and Bullock, 2013; Schrader et al., 2015) appears to have experienced the most Cr-mobilization. However, shock-heated GRO 03116 (Alexander et al., 2013; Schrader et al., 2015) does not plot near GRA 06100; it is intermediate in terms of Cr_2O_3 compared to the other CR chondrites studied here (Table 1; Fig. 1). Despite appearing almost identical to GRA 06100 in terms of bulk H-isotopic composition and bulk C/H ratio (Fig. 2), GRO 03116 appears to be less shocked in terms of H, C, N abundances and N-isotopic composition (Alexander et al., 2013). The difference between the Cr-compositions of GRA 06100 and GRO 03116 likely results from the exsolution of Cr being a diffusive process that depends upon thermal history; type of heating (radiogenic or impact-driven), duration of heating, and peak metamorphic temperature. The difference in Cr_2O_3 contents of ferroan olivine between the two shock-heated CR chondrites likely results from GRO 03116 being less shock-modified (i.e., it experienced a lower peak temperature and/or shorter duration heating) than GRA 06100, which is consistent with various mineralogical observations that will be discussed later.

The similarity in the ferroan olivine Cr data between shock-heated GRO 03116 and unshocked CR chondrites demonstrates that two chondrites that appear to plot close to one another may have experienced different overall thermal histories. Thus, while this technique is useful for identifying metamorphic end-members (only the most shocked samples exhibit significant Cr-mobilization), it is not able to identify moderately shocked CR chondrites and should be used to complement other methods when quantifying the degree of heating (either radiogenic or shock-driven) experienced by a sample.

When compared with data from 15 other CR chondrites (Abreu and Brearley, 2010; Berlin, 2009; and recalculated data of Schrader et al., 2015), MIL 090657 appears to be less heated than all CR chondrites other than MET 00426 (Berlin, 2009) and QUE 99177 (Abreu and Brearley, 2010) (Fig. 1). Data for MET 00426 and QUE 99177 vary between studies (i.e., Berlin, 2009 and Abreu and Brearley, 2010 *vs.* the recalculated values from Schrader et al., 2015; Fig. 1). In the case of MET 00426, this is likely due to the low number of analyses (five) presented in Schrader et al. (2015). It is also difficult to compare between different studies as the number of analyses are not provided and consistency is required; a suitable number of analyses must be performed (approximately $n = 50$) to ensure data are representative and analyses must be performed on grain cores and not elsewhere in the olivine grain (i.e., rim or the transition between core and rim). There is no apparent relationship between the Cr-content of ferroan olivine in CR chondrites and the degree of aqueous alteration they have experienced. This is likely because the temperature of aqueous alteration was very low (<88 °C; Jilly-Rehak et al., 2018) and was decoupled from any heating that was significant enough to alter silicates. Regardless, MIL 090657 appears to have experienced very minimal, if any, thermal metamorphism.

Overall, the minimally heated nature of the CR chondrites is reflected by the spread of Cr_2O_3 compositions, which does not exhibit turn over like in the UOC and CO chondrites (Fig. 1; Grossman and Brearley, 2005; Davidson et al., 2014b). This suggests that the majority of the CR chondrites do not exceed a thermal metamorphic subtype of 3.1 (Schrader et al., 2015), while their organics indicate that they experienced lower temperature conditions than CO and LL chondrites of petrologic type 3.0 and possibly all CI and CM chondrites (Alexander et al., 2013). With the exception of the shock-heated samples GRA 06100 and GRO 03116, the spread in Cr_2O_3 data is most likely due to the unaltered nature of the majority of CR chondrites (i.e., heterogeneous mineral compositions have not been homogenized), and because FeO-rich chondrules in the various CR chondrites have distinct minor element compositions from one another – more so than observed in other chondrite groups (see discussion and Figs. 7c and 8e in Schrader et al., 2015).

4.2. Primary vs. secondary signatures

4.2.1. Measures of pristinity: Bulk meteorite and IOM

The bulk elemental composition of MIL 090657 indicates that it is of petrologic type 2.7 according to the scheme of Alexander et al. (2013). This would suggest that MIL 090657 is more pristine than all other CR chondrites analyzed to date (Fig. 2). Based on their bulk isotopic compositions, MET 00426 and QUE 99177 have petrologic types 2.6 and 2.4, respectively (Alexander et al., 2013). In contrast, the C and N contents of bulk GRA 06100 and GRO 03116 are much lower than for typical CRs, consistent with significant heating (Alexander et al., 2013). If the temperatures reached during shock were high enough to break down phyllosilicates or dehydrate amorphous silicates, H would be preferentially lost resulting in higher H isotopic compositions (i.e., higher δD). The fact that MIL 090657 falls somewhat below the best fit line to the literature CR data (Fig. 2) could be due to the addition of water/OH and/or isotopic exchange during Antarctic weathering (Alexander et al., 2013).

Position sensitive X-ray diffraction data indicate that MIL 090657 contains only ~6 vol.% phyllosilicate and 11 vol.% Fe-bearing amorphous material (Howard et al., 2015b). This is similar to CR chondrite Lapaz Icefield 02342, which is considered to be of petrologic type 2.7 based on phyllosilicate fraction (Howard et al., 2015a), though the low abundance of presolar silicates in this meteorite suggests that it may in fact be more altered (Nittler et al., 2019). The high abundance of amorphous material and low abundance of phyllosilicate further supports the minimally aqueously altered nature of MIL 090657.

GRA 06100 is estimated to be a type 2.8 according to the scheme of Howard et al. (2015a); 11.4 vol.% total phyllosilicate, 5.8 vol.% Fe-rich amorphous material. The discrepancy between the assignment of type 2.8 for GRA 06100 and type 2.7 for MIL 090657 according to the scheme of Howard et al. (2015a) is probably due to the lower phyllosilicate fraction of GRA 06100 resulting from dehydration during shock heating. GRO 03116, which has a high

weathering grade of B/C, contains abundant amorphous material that is inferred to be mainly rust, and is estimated to be a type 2.5 (Howard et al., 2015a).

The IOM extracted from MIL 090657 has C-, N- and H-isotopic compositions (e.g., Fig. EA-3) that are similar to other CR chondrites (Alexander et al., 2007). However, the yield of IOM from MIL 090657 was low, accounting for only 0.236 wt.% C or ~20% of the bulk C. As discussed by Alexander et al. (2015, 2017), the IOM isolated from chondrites typically only accounts for ~50% of the bulk C, and the nature of the C that is unaccounted for remains undetermined. Why the IOM yield from MIL 090657 is particularly low is unclear; it could be analytical artifact or a hint that the unidentified carbonaceous material is more abundant in more primitive chondrites.

4.2.2. Fe,Ni metal and sulfide compositions

The relationship between Co and Ni abundances in Fe, Ni metal is a sensitive indicator of the degree of thermal metamorphism experienced by a host meteorite in its parent body; a positive relationship indicates no noticeable heating (type ≪3.05), while an inverse or no relationship indicates thermal alteration above a type 3.05 (Kimura et al., 2008). The Ni-rich metal in MIL 090657 is enriched in Co relative to Ni-poor metal (Fig. 5), indicating MIL 090657 was not thermally metamorphosed. This positive Co vs. Ni relationship is exhibited by Fe,Ni metal in other unmetamorphosed CR chondrites, including MET 00426 and QUE 99177 (Schrader et al., 2015). In contrast, the Fe,Ni metal in GRA 06100 exhibits an inverse relationship between Co and Ni (Abreu and Bullock, 2013; Schrader et al., 2015), indicating that it has undergone noticeable shock-driven modification.

While it is not possible to determine the overall Co/Ni trend for metal in GRO 03116 as only Ni-poor metal has been identified in this heavily weathered chondrite (Schrader et al., 2015), it is possible to compare Ni-poor metal that may still be diagnostic of significant heating. The Co/Ni ratio of Ni-poor metal in GRO 03116 (0.04–0.06 wt.% ratio; Schrader et al., 2015) is more similar to that of Ni-poor metal in MIL 090657 (0.02–0.06 wt.% ratio) than GRA 06100 (0.08–0.11 wt.% ratio), further suggesting that GRO 03116 is not as shock-heated as GRA 06100.

The morphologies, mineralogies, and compositions of sulfide assemblages within chondrites are not only indicators of the conditions of their formation, but also of their parent body modification. Their morphologies indicate whether they formed by low-temperature aqueous alteration or solid state exsolution (either at high or low temperature); pentlandite lamellae within pyrrhotite indicate solid state exsolution and are inconsistent with formation via aqueous alteration. The sulfides in MIL 090657 consist entirely of pyrrhotite and pentlandite (often in complex intergrowths with pentlandite lamellae surrounded by pyrrhotite; Fig. 4b) that are sometimes associated with Ni-rich metal, and are similar to assemblages from other pristine CR chondrites (Schrader et al., 2008, 2015). Highly aqueously altered CR chondrites, such as Renazzo and Al Rais, contain magnetite-bearing sulfide assemblages (Schrader et al., 2015); no magnetite was observed in MIL 090657 chondrules (though minor magnetite framboids were noted in the matrix; Schrader et al., 2014), indicating that MIL 090657 is not significantly aqueously altered.

Since sulfide assemblages in CR2 and so-called CR3 chondrite chondrules formed via cooling from a melt and not via aqueous alteration (Schrader et al., 2015), the compositions of their pentlandite-pyrrhotite intergrowths are dictated by their high temperature closure temperatures. Using geothermometry, the Fe-Ni-S compositions of pentlandite-pyrrhotite intergrowths in MIL 090657 indicate that they equilibrated below 600 °C, at approximately 500 °C (Fig. 6). This is inconsistent with their formation during parent body alteration, but suggests cooling from high temperature (i.e., after chondrule formation; Schrader et al., 2015, 2018b). Therefore, the compositions and morphologies of sulfides in MIL 090657 indicate that this meteorite has not experienced significant thermal or aqueous alteration.

The shock-heated CR chondrite GRA 06100 contains complex intergrowths of Fe,Ni metal and pyrrhotite. It does not contain pentlandite, which is necessary for plotting on isothermal phase diagrams, preventing equilibration temperatures from being determined. Abreu and Bullock (2013) suggested that the lack of pentlandite is due to GRA 06100 being briefly heated to temperatures in excess of ~600 °C during an impact event. Such a heating event would have caused any pre-existing pentlandite and pyrrhotite to decompose into a monosulfide solid solution, which upon rapid cooling below ~600 °C did not re-exsolve into pentlandite and pyrrhotite, but instead a mixture of pyrrhotite, kamacite, and Ni-Co-rich metal (Kimura et al., 2011; Abreu and Bullock, 2013). Conversely, GRO 03116 does contain pentlandite (Schrader et al., 2015), indicating that it is not as shocked as GRA 06100.

4.2.3. Chondrule silicate compositions

The ratios of Fe# of olivine to the Fe# of LCP for individual chondrules, reflect the degree of parent body thermal metamorphism a chondrite has experienced (Tenner et al., 2015; Schrader et al., 2017). Since olivine and pyroxene have different Fe-Mg diffusion rates (Ganguly and Tazzoli, 1994; Chakraborty, 1997), pyroxene has lower Fe contents (i.e., lower Fe#) than olivine (i.e., relatively higher Fe#) in thermally altered chondrites (e.g., Wlotzka, 2005). Chondrule data from MIL 090657 show nearly a 1:1 Fe# ratio within 1σ error (Table 4), as do other relatively unaltered CR2 chondrites (Tenner et al., 2015; Schrader et al., 2017), indicating that MIL 090657 was not noticeably thermally metamorphosed. In contrast, chondrule data from GRA 06100 typically show a large deviation from the 1:1 relationship (Table 4), in agreement with the conclusion that GRA 06100 has been heated (Abreu and Bullock, 2013; Alexander et al., 2013; Schrader et al., 2015; this study). As solid-state Fe-Mg interdiffusion is faster in olivine than in LCP (e.g., Huebner and Nord, 1981; Benedix et al., 1998), chondrules in GRA 06100 most likely exhibit Fe# of olivine > Fe# of LCP because of oxidation of Fe during heating.

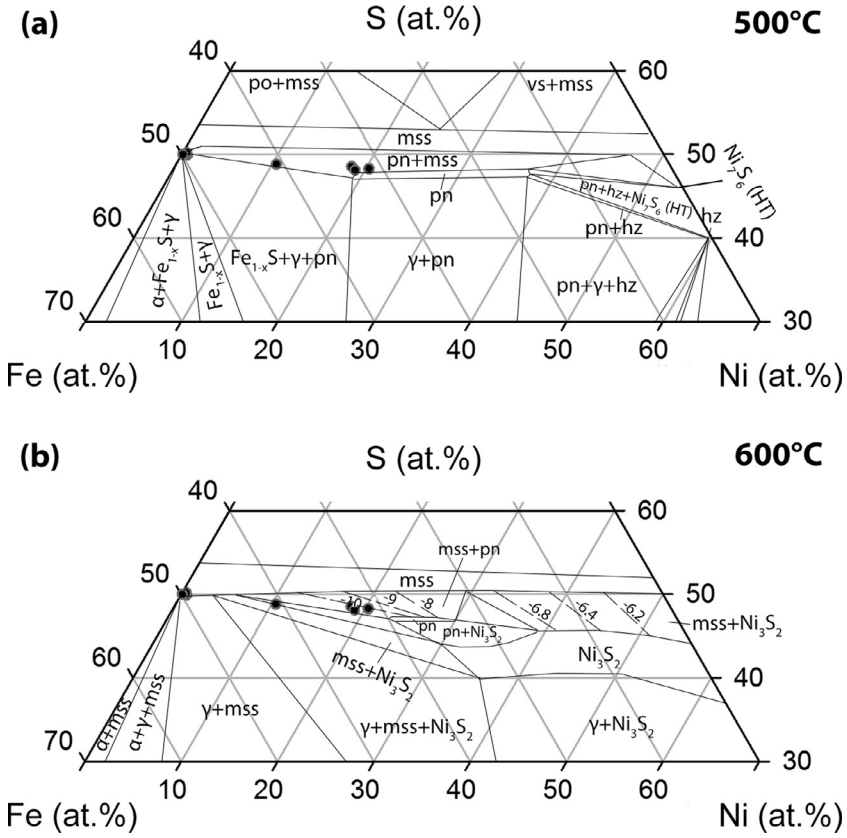

Fig. 6. Sulfide compositional data for MIL 090657,6 superimposed on Fe-Ni-S isothermal phase diagrams at (a) 500 °C and (b) 600 °C. Sulfides are consistent with equilibrating around 500 °C, as pentlandite is near the pentlandite stability field in the 500 °C phase diagram (a) and the troilite analyses connect to the pentlandite field along the tie line. In contrast, pentlandite is too Ni-poor to have equilibrated at 600 °C (b). Where po = pyrrhotite, pn = pentlandite, mss = monosulfide solid solution, hz = heazlewoodite (Ni_3S_2), vs = vaesite (NiS_2), vio = violarite (Ni_3S_4), α = kamacite, and γ = taenite. Phase diagrams are adapted from Raghavan (2004) with original data from (a) Shewman and Clark (1970) and (b) Kosyakov et al. (2003).

Anomalous lunar plagioclase stoichiometries compared to terrestrial plagioclase stoichiometries have been attributed to the presence of "excess silica" denoted as [ ]Si_4O_8 (Beaty and Albee, 1980). Experiments show that, at temperatures of 1200–1500 °C and 1 atm pressure under anhydrous conditions, plagioclase can incorporate up to 10 wt. % silica (Longhi and Hays, 1979). Silica excesses have been reported for chondrule plagioclase from low petrologic type chondrites (Tenner et al., 2014, Chaumard et al., 2017; Tenner, 2017; Davidson et al., 2019). Carbonaceous chondrites of petrologic types CO3.05–3.1 and CV3.1 exhibit systematically lower [ ]Si_4O_8 and An# compared to the more primitive ungrouped Acfer 094 and CR chondrites (Chaumard et al., 2017). Thus, determining [ ]Si_4O_8 in chondrule plagioclase may be used to assess the degree of re-heating experienced by chondrules from low petrologic type chondrites either in the nebula or in their parent bodies (e.g., Tenner et al., 2014, Chaumard et al., 2017; Tenner, 2017; Davidson et al., 2019).

Calculated [ ]Si_4O_8 for plagioclase in six chondrules ranges from –0.48 mol.% to 9.6 mol.%; plagioclase in five of six chondrules show resolvable excess silica. While it is possible that not all chondrule plagioclase takes on excess silica, the chondrules analyzed here in MIL 090657 exhibit a range of excess silica similar to that seen in the CR chondrite QUE 99177 (up to 10.3 mol.%; Tenner et al., 2014) but greater than that exhibited by plagioclase in the CR chondrite MET 00426 (up to 6.4 mol.%; Tenner et al., 2014) and the primitive CO chondrite DOM 08006 (up to 6.9 mol.%; Davidson et al., 2019). Despite being based on limited statistics, these results indicate that most MIL 090657 chondrules experienced minimal reprocessing in the nebula and the parent body and further demonstrate the pristine nature of MIL 090657.

4.2.4. Presolar grains

Presolar grains provide another parameter for testing the degree of parent body aqueous alteration and/or thermal metamorphism of a given sample (e.g., Nguyen et al., 2007, 2010; Floss and Stadermann, 2009a,b, 2012; Vollmer et al., 2009; Davidson et al., 2010, 2014a,b,c; Zhao et al., 2011, 2013; Leitner et al., 2012, 2016; Haenecour et al., 2018; Nittler et al., 2018). The O-anomalous (silicate and oxide) presolar grain abundance of ~ 112 ± 25 ppm (n = 27) for MIL 090657 matrix is similar to the abundances reported for the CR2 chondrite Northwest Africa (NWA) 852 (116 ppm; Leitner et al., 2012), but not as high as those in MET 00426

(~180 ppm; Floss and Stadermann, 2009b; Leitner et al., 2016) and QUE 99177 (~190 ppm; Floss and Stadermann, 2009b; Nguyen et al., 2010) (Fig. 7). However, this may be due to matrix heterogeneity; QUE 99177 shows considerable heterogeneity in the distribution of O-anomalous presolar grains with comparably-sized areas yielding vastly different abundances of 90 ± 50 ppm (~3100 μm^2) and 335 ± 75 ppm (~3400 μm^2) (Floss and Stadermann, 2009b). The overall QUE 99177 abundance used here was determined from a larger matrix area (~29,700 μm^2; data were combined from the studies of Floss and Stadermann, 2009b; Nguyen et al., 2010) than that analyzed here (~12,000 μm^2). No such heterogeneity has been reported for MET 00426, though less area has been analyzed (~15,000 μm^2; data combined from Floss and Stadermann, 2009b; Leitner et al., 2016).

Presolar SiC abundances were not affected by aqueous alteration at the low temperatures experienced by the CR chondrite parent body, <88 °C (Jilly-Rehak et al., 2018), but are affected by heating in other carbonaceous chondrite groups (Davidson et al., 2014a). The high abundance of presolar SiC grains in MIL 090657 matrix, 40 ± 20 ppm ($n = 6$), which agrees with abundances reported for CRs of all petrologic types and other primitive chondrites (e.g., Davidson et al., 2014a; Fig. 7), indicates that this sample was minimally heated, if at all, on the CR chondrite parent body.

4.2.5. Physical processing

MIL 090657,6 displays linear foliation (Fig. EA-1), where chondrules exhibit elongated, slightly flattened morphologies that align in a common direction. This indicates

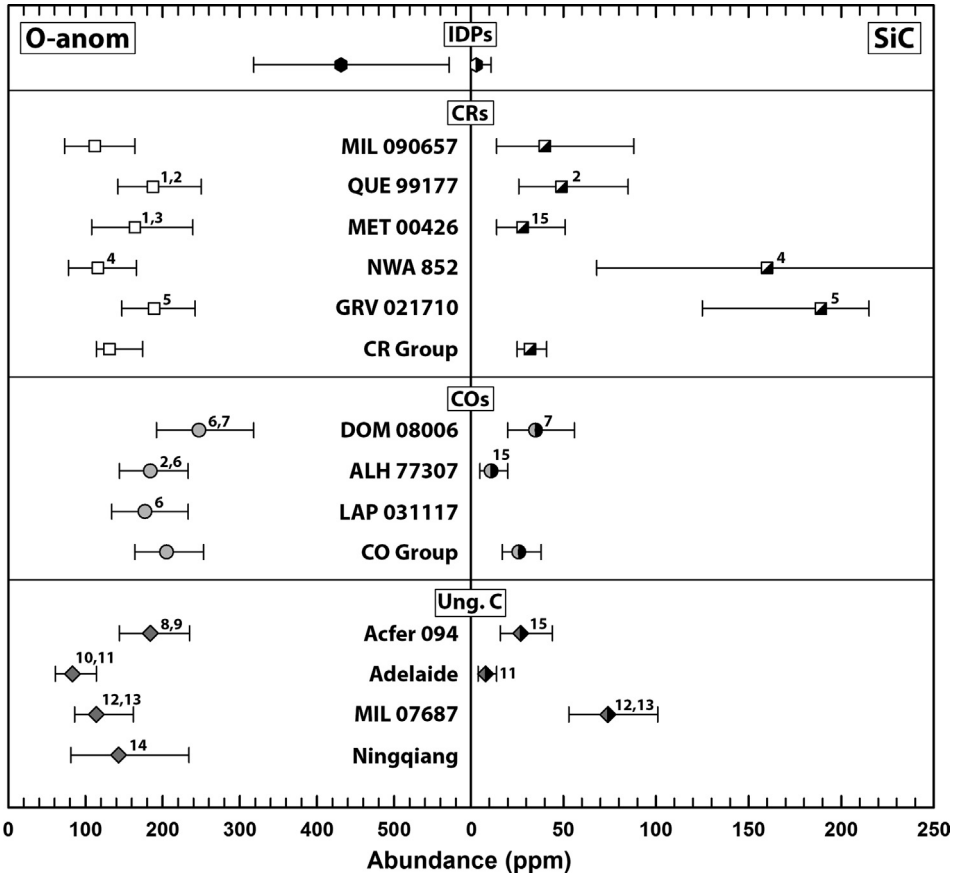

Fig. 7. Presolar O-anomalous (combined silicate and oxide) and SiC presolar grain abundances for MIL 090657 compared to interplanetary dust particles (IDPs) and CR, CO, and ungrouped carbonaceous (Ung. C) chondrites. The IDP abundances are the average area-weighted presolar abundances based on 50 O-anomalous grains (~430 + 140/–113 ppm) and 2 SiC grains (~2 + 8/–3 ppm) found in 44 IDPs across 8 studies (see Appendix in Alexander et al., 2017 and references therein). Both O-anomalous and SiC abundances for MIL 090657 are from this study; data from other meteorites are drawn from other, often multiple, sources. Where data exist for the same meteorite from multiple studies, the data have been combined for clarity and to reduce errors associated with counting statistics. All errors shown are 2σ and, as the method used for determining errors varies between studies, all were recalculated here using the Poisson distribution of counting statistics (Gehrels, 1986). The group abundances are averages determined from the cited studies, with the exception of the CR chondrite group SiC abundance, which is from the larger data set of Davidson et al. (2014b). Data sources are as follows: [1]Floss and Stadermann (2009b), [2]Nguyen et al. (2010), [3]Leitner et al. (2016), [4]Leitner et al. (2012), [5]Zhao et al. (2013), [6]Haenecour et al. (2018), [7]Nittler et al. (2018), [8]Nguyen et al. (2007), [9]Vollmer et al. (2009), [10]Davidson et al. (2010), [11]Floss and Stadermann (2012), [12]Davidson et al. (2015b), [13]Floss and Brearley (2015), [14]Zhao et al. (2011), and [15]Davidson et al. (2014a).

that they have experienced some type of physical processing. Foliation of chondrules has previously been observed in both ordinary and carbonaceous chondrites, and has been variably attributed to: (1) deposition during accretion (Dodd, 1965), (2) compaction due to overburden pressure on the parent body (Cain et al., 1986), and (3) shock-impact driven compaction (e.g., Scott et al., 1992; Rubin, 2012; Hanna et al., 2015; Lindgren et al., 2015; Charles et al., 2018).

If the linear foliation in MIL 090657 resulted from deposition during accretion of the CR chondrite parent body, such foliation should be observed in most, if not all, CR chondrites. While linear foliation has been noted in the CR chondrite NWA 801 (Charles et al., 2018), none was observed in a study of 15 CR chondrites (including a different thin section of NWA 801, though this may be a thin-sectioning artifact; Schrader et al., 2015), suggesting that such foliation is rare in this meteorite group and is not a depositional feature.

Explaining the genesis of foliation via overburden compaction requires that MIL 090657 was buried more deeply in the CR chondrite parent body than CR chondrites that do not display foliation. Noble gas studies have shown that MIL 090657 does not exhibit evidence for solar wind exposure, suggesting that this meteorite does not originate from the upper most layers of the CR parent body (Busemann et al., 2016; Roth and Leya, 2018), supporting the idea that MIL 090657 was buried at depth. However, overburden compaction that was significant enough to foliate chondrules, even over long timescales, should result in some degree of heating (e.g., Cain et al., 1986), but there is no evidence for heating of the silicate and opaque phases in MIL 090657. Therefore, the foliation seen in MIL 090657 is not likely explained by overburden compaction.

Energetic impacts should also lead to heating of various chondritic components. Organic matter tends to be a more sensitive indicator of thermal metamorphism than silicate or opaque minerals (e.g., Alexander et al., 2007, 2010; Busemann et al., 2007); the H/C ratio of shock-heated CM chondrites is lower than that of non-shocked CM chondrites (Alexander et al., 2007, 2010). The H/C ratio of IOM extracted from MIL 090657 is higher than that of other CR chondrites (Alexander et al., 2017), consistent with it not being shock-heated. The lack of both shock features and evidence for heating in MIL 090657 eliminates the possibility that the observed foliation results from a single energetic impact. Furthermore, GRA 06100 experienced brief impact-driven shock metamorphism (e.g., Abreu and Bullock, 2013), but does not display linear foliation, suggesting that the formation of this feature in the CR chondrites is not definitively indicative of impact processing.

To explain linear foliation observed in the CR2 NWA 801, Charles et al. (2018) speculated that many CR chondrite chondrules likely formed as ellipsoids and that post-accretional impacts could have deformed hydrated and porous material on the CR chondrite parent body, resulting in apparent foliation. This could account for the presence of linear foliation in NWA 801 and a lack of evidence of heating (Charles et al., 2018). Similarly, foliated chondrules have been observed in unheated CM chondrites (e.g., Rubin, 2012; Lindgren et al., 2015), which also contain open or secondary-mineral filled fractures in the matrix that are dominantly parallel and/or perpendicular to the foliated chondrules. Multiple low-energy shock events were proposed to explain the presence of deformed chondrules and fracturing in the absence of heating (Lindgren et al., 2015). MIL 090657 does not exhibit fractures, either preferentially parallel or perpendicular to the foliated chondrules (EA-1), to support a history of impacts. However, the CM chondrites may be more prone to fracturing as they are more friable than CR chondrites.

Though it is not possible to come to a definitive conclusion, it is perhaps most likely that the linear foliation in MIL 090657 results from a low energy impact(s) that compacted hydrated, porous material, and so did not result in any detectable heating. In contrast, GRA 06100 likely represents material that was closer to an impact site in the CR chondrite parent body.

5. SUMMARY

In this study we have used a number of techniques to constrain the degree of thermal and aqueous alteration recorded by MIL 090657, and found that MIL 090657 is a very pristine CR2.7 carbonaceous chondrite (according to the scheme of Alexander et al., 2013) that has experienced very minimal (if any) thermal or aqueous processing. The identification of MIL 090657 as a minimally altered CR chondrite of relatively high mass at 133.1 g, makes it an ideal target for a multitude of studies, which is important given the dwindling supplies of the most pristine CR chondrites.

In comparison, GRA 06100 appears to be the most thermally metamorphosed CR chondrite analyzed to date, as reflected by bulk isotopic compositions, the Cr_2O_3-content of its ferroan olivine, Co/Ni ratios of its Fe,Ni metal, and the Fe# of olivine and low-calcium pyroxene of its chondrules. Combined, these petrographic characteristics provide useful indicators for determining the relative pristinity/degree of heating of low petrographic (type 1–3) chondrites.

ACKNOWLEDGEMENTS

We thank Ken Domanik (UA), Tim Rose, Emma Bullock, and Steve Lynton (SI), and J.T. Armstrong (CIW) for assistance with the electron microprobes. This manuscript was significantly improved by helpful reviews from Alan Rubin, Travis Tenner, an anonymous reviewer, and the editorial expertise of AE Sara Russell. US Antarctic meteorite samples are recovered by the Antarctic Search for Meteorites (ANSMET) program, which has been funded by NSF and NASA, and characterized and curated by the Department of Mineral Sciences of the Smithsonian Institution and the Astromaterials Acquisition and Curation Office at NASA Johnson Space Center. This work was funded by NASA grants NNX11AG67G (PI: CMODA), NNX10AI63G and NNX11AB40G (PI: LRN), and NNX17AE53G (PI: DLS), and the Arizona State University Center for Meteorite Studies.

APPENDIX A. SUPPLEMENTARY MATERIAL

Supplementary data to this article can be found online at https://doi.org/10.1016/j.gca.2019.09.033.

REFERENCES

Abreu N. M. and Brearley A. J. (2010) Early solar system processes recorded in the matrices of two highly pristine CR3 carbonaceous chondrites, MET 00426 and QUE 99177. *Geochim. Cosmochim. Acta* **74**, 1146–1171.

Abreu N. M. and Bullock E. (2013) Opaque assemblages in CR2 Graves Nunataks (GRA) 06100 as indicators of shock-driven hydrothermal alteration in the CR chondrite parent body. *Meteorit. Planet. Sci.* **48**, 2406–2429.

Alexander C. M. O'D., Fogel M., Yabuta H. and Cody G. D. (2007) The origin and evolution of chondrites recorded in the elemental and isotopic compositions of their macromolecular organic matter. *Geochim. Cosmochim. Acta* **71**, 4380–4403.

Alexander C. M. O'D., Newsome S. D., Fogel M. L., Nittler L. R., Busemann H. and Cody G. D. (2010) Deuterium enrichments in chondritic macromolecular material –Implications for the origin and evolution of organics, water and asteroids. *Geochim. Cosmochim. Acta* **74**, 4417–4437.

Alexander C. M. O'D., Bowden R., Fogel M. L., Howard K. T., Herd C. D. K. and Nittler L. R. (2012) The provenances of asteroids, and their contributions to the volatile inventories of the terrestrial planets. *Science* **337**, 721–723.

Alexander C. M. O'D., Howard K. T., Bowden R. and Fogel M. L. (2013) The classification of CM and CR chondrites using bulk H, C, and N abundances and isotopic compositions. *Geochim. Cosmochim. Acta* **123**, 244–260.

Alexander C. M. O'D., Bowden R., Fogel M. L. and Howard K. T. (2015) Carbonate abundances and isotopic compositions in chondrites. *Met. Planet. Sci.* **50**, 810–833.

Alexander C. M. O'D., Cody G. D., De Gregorio B. T., Nittler L. R. and Stroud R. M. (2017) The nature, origin and modification of insoluble organic matter in chondrites, the major source of Earth's C and N. *Chem. Erde* **77**, 227–256.

Beaty D. W. and Albee A. L. (1980) Silica solid solution and zoning in natural plagioclase. *Am. Mineral.* **65**, 63–74.

Benedix G. K., McCoy T. J., Keil K., Bogard D. D. and Garrison D. H. (1998) A petrologic and isotopic study of winonaites: evidence for early partial melting, brecciation, and metamorphism. *Geochim. Cosmochim. Acta* **62**, 2535–2553.

Berlin J. (2009) Mineralogy and bulk chemistry of chondrules and matrix in petrologic type 3 chondrites: Implications for early solar system processes. Ph.D thesis. University of, New Mexico, Albuquerque, New Mexico, USA.

Busemann H., Alexander C. M. O'D. and Nittler L. R. (2007) Characterization of insoluble organic matter in primitive meteorites by microRaman spectroscopy. *Meteorit. Planet. Sci.* **42**, 1387–1416.

Busemann H., Kuga M., Spring N. H., Schrader D. L., Holinger S., Maden C. and Fehr M. A. (2016) Noble gases in CR chondrites: the primordially trapped inventory and records of parent body, space and terrestrial processing. *Developments in Noble Gas Understanding and Expertise 4, Nancy (abstr.)*.

Cain P. M., McSween, Jr., H. Y. and Woodward N. B. (1986) Structural deformation of the Leoville chondrite. *Earth Planet. Sci. Lett.* **77**, 165–175.

Chakraborty S. (1997) Rates and mechanisms of Fe-Mg interdiffusion in olivine at 980–1300°C. *J. Geophys. Res.* **102**, 12317–12331.

Charles C. R. J., Robin P.-Y., Davis D. W. and McCausland P. J. A. (2018) Shapes of chondrules determined from the petrofabric of the CR2 chondrite NWA 801. *Meteorit. Planet. Sci.* **53**, 935–951.

Chaumard N., Hertwig A. T., Kita N. T., Tenner T. J. and Kimura M. (2017) Measurements of silica excess in plagioclase in chondrules from primitive carbonaceous chondrites: Implications for ^{26}Al–^{26}Mg systematics. *80th Annual Meeting of the Meteoritical Society, #6309 (abstr.)*.

Davidson J., Busemann H., Franchi I. A. and Grady M. M. (2010) Presolar grain inventories of the ungrouped C3 Adelaide and the CV3 RBT 04133. *Lunar Planet. Sci. XLI. #2230 (abstr.)*.

Davidson J., Busemann H., Nittler L. R., Alexander C. M. O. 'D., Orthous-Daunay F.-R., Franchi I. A. and Hoppe P. (2014a) Abundances of presolar silicon carbide grains in primitive meteorites determined by NanoSIMS. *Geochim. Cosmochim. Acta* **139**, 248–266.

Davidson J., Nittler L. R., Alexander C. M. O'D. and Stroud R. M. (2014b) Petrography of very primitive CO3 chondrites: Dominion Range 08006, Miller Range 07687, and four others. *Lunar Planet. Sci. XLV. #1384 (abstr.)*.

Davidson J., Schrader D. L., Busemann H., Franchi I. A., Connolly, Jr., H. C., Lauretta D. S., Alexander C. M. O'D., Verchovsky A. and Greenwood R. C. (2014c) Petrography, stable isotope compositions, microRaman spectroscopy and presolar components of Roberts Massif 04133: a reduced CV3 carbonaceous chondrite. *Met. Planet. Sci.* **49**, 2133–2151.

Davidson J., Alexander C. M. O'D., Schrader D. L., Nittler L. R. and Bowden R. (2015a) Miller Range 090657: a very pristine Renazzo-like (CR) carbonaceous chondrite. *Lunar Planet. Sci. XLVI. #1603 (abstr.)*.

Davidson J., Nittler L. R., Stroud R. M., Takigawa A., De Gregorio B. T., Alexander C. M. O'D., Kilcoyne A. L. D. and Cody G. D. (2015b) Organic matter in the unique carbonaceous chondrite Miller Range 07687: a coordinated in situ NanoSIMS, FIB-TEM, and XANES study. *Lunar Planet. Sci. XLVI. #1609 (abstr.)*.

Davidson J., Alexander C. M. O'D., Stroud R. M., Busemann H. and Nittler L. R. (2019) Mineralogy and petrology of Dominion Range 08006: A very primitive CO_3 carbonaceous chondrite. *Geochim. Cosmochim. Acta* **265**, 259–278.

Defouilloy C., Nakashima D., Joswiak D. J., Brownlee D. E., Tenner T. J. and Kita N. T. (2017) Origin of crystalline silicatesfrom comet 81P/Wild 2: combined study on their oxygen isotopes and mineral chemistry. *Earth Planet. Sci. Lett.* **465**, 145–154.

Dodd Jr R. T. (1965) Preferred orientation of chondrules in chondrites. *Icarus* **4**, 308–316.

Floss C. and Brearley A. J. (2015) Effects of secondary processing on presolar grain abundances and compositions in the unique carbonaceous chondrite Miller Range 07687. *Lunar Planet. Sci. XLVI. #1004 (abstr.)*.

Floss C. and Stadermann F. (2009a) High abundances of circumstellar and interstellar C-anomalous phases in the primitive CR3 chondrites QUE 99177 and MET 00426. *Astrophys. J.* **697**, 1242–1255.

Floss C. and Stadermann F. J. (2009b) Auger Nanoprobe analysis of presolar ferromagnesian silicate grains from primitive CR chondrites QUE 99177 and MET 00426. *Geochim. Cosmochim. Acta* **73**, 2415–2440.

Floss C. and Stadermann F. J. (2012) Presolar silicate and oxide abundances and compositions in the ungrouped carbonaceous chondrite Adelaide and the K chondrite Kakangari: the effects of secondary processing. *Met. Planet. Sci.* **47**, 992–1009.

Floss C., Le Guillou C. and Brearley A. (2014) Coordinated NanoSIMS and FIB-TEM analyses of organic matter and associated matrix materials in CR3 chondrites. *Geochim. Cosmochim. Acta* **139**, 1–25.

Frank D. R., Zolensky M. E. and Le L. (2014) Olivine in terminal particles of Stardust aerogel tracks and analogous grain in chondrite matrix. *Geochim. Cosmochim. Acta* **142**, 240–259.

Ganguly J. and Tazzoli V. (1994) Fe^{2+}-Mg interdiffustion in orthopyroxene: Retrieval from the data on intracrystalline exchange reaction. *Am. Mineral.* **79**, 930–937.

Gehrels N. (1986) Confidence limits for small numbers of events in astrophysical data. *Astrophys. J.* **303**, 336–346.

Grossman J. N. and Brearley A. J. (2005) The onset of metamorphism in ordinary and carbonaceous chondrites. *Meteorit. Planet. Sci.* **40**, 87–122.

Haenecour P., Floss C., Zega T. J., Croat T. K., Wang A., Jolliff B. L. and Carpenter P. (2018) Presolar silicates in the matrix and fine-grained rims around chondrules in primitive CO3.0 chondrites: Evidence for pre-accretionary aqueous alteration of the rims in the solar nebula. *Geochim. Cosmochim. Acta* **221**, 379–405.

Hanna R. D., Ketcham R. A., Zolensky M. and Behr W. M. (2015) Impact-induced brittle deformation, porosity loss, and aqueous alteration in the Murchison CM chondrite. *Geochim. Cosmochim. Acta* **171**, 256–282.

Howard K. T., Alexander C. M. O'D., Schrader D. L. and Dyl K. A. (2015a) Classification of hydrous meteorites (CR, CM and C2 ungrouped) by phyllosilicate fraction: PSD-XRD modal mineralogy and planetesimal environments. *Geochim. Cosmochim. Acta* **149**, 206–222.

Howard K. T., Davidson J., Alexander C. M. O'. D. and Abreu N. M. (2015b) The glue that holds worlds together: Abundance, origin and significance of amorphous Fe, Mg silicate in carbonaceous chondrites. *Lunar Planet. Sci. XLVI. #2244 (abstr.)*.

Huebner J. S. and Nord, Jr, G. L. (1981) Assessment of diffusion in pyroxene: What we do and do not know. *Lunar Planet. Sci. XII. #479–481 (abstr.)*.

Jilly-Rehak C. E., Huss G. R., Nagashima K. and Schrader D. L. (2018) Low temperature aqueous alteration on the CR chondrite parent body: Implications from in situ oxygen isotopes. *Geochim. Cosmochim. Acta* **222**, 230–252.

Jones R. H. (2012) Petrographic constraints on the diversity of chondrule reservoirs in the protoplanetary disk. *Meteorit. Planet. Sci.* **47**, 1176–1190.

Kimura M., Grossman J. N. and Weisberg M. K. (2008) Fe-Ni metal in primitive chondrites: Indicators of classification and metamorphic conditions for ordinary and CO chondrites. *Meteorit. Planet. Sci.* **43**, 1161–1177.

Kimura M., Grossman J. N. and Weisberg M. K. (2011) Fe- Ni metal and sulfide minerals in CM chondrites: an indicator for thermal history. *Meteorit. Planet. Sci.* **46**, 431–442.

Kosyakov V. I., Sinyakova E. F. and Shestakov V. A. (2003) Dependence of sulfur fugacity on the composition of phase associations in the Fe–FeS–NiS–Ni system at 873 K. *Geochem. Int.* **7**, 660–669.

Le Guillou C. and Brearley A. J. (2014) Relationships between organics, water and early stages of aqueous alteration in the pristine CR3.0 chondrite MET 00426. *Geochim. Cosmochim. Acta* **131**, 344–367.

Leitner J., Vollmer C., Hoppe P. and Zipfel J. (2012) Characterization of presolar material in the CR chondrite Northwest Africa 852. *Astrophys. J.* **745**, 38–53.

Leitner J., Vollmer C., Floss C., Zipfel J. and Hoppe P. (2016) Ancient stardust in fine-grained chondrule dust rims from carbonaceous chondrites. *Earth Planet. Sci. Lett.* **434**, 117–128.

Lindgren P., Hanna R. D., Dobson K. J., Tomkinson T. and Lee M. R. (2015) The paradox between low shock-stage and evidence for compaction in CM carbonaceous chondrites explained by multiple low-intensity impacts. *Geochim. Cosmochim. Acta* **148**, 159–178.

Lodders K., Palme H. and Gail H.-P. (2009) Abundances of the elements of the solar system. In *The Landolt-Bornstein Database* (ed. J. E. Trümper). Springer, Berlin, pp. 560–598.

Longhi J. and Hays J. F. (1979) Phase equilibria and solid solution along the join $CaAl_2Si_2O_8$–SiO_2.Am. *J. Sci.* **279**, 876–890.

Martins Z., Alexander C. M. O'D., Orzechowska G. E., Fogel M. L. and Ehrenfreund P. (2007) Indigenous amino acids in primitive CR meteorites. *Meteorit. Planet. Sci.* **42**, 2125–2136.

McBride K., Satterwhite C. and Righter K. (2013) US Antarctic CR chondrites: A limited resource providing material for a broad array of planetary sciences. *Lunar Planet. Sci. XLIV. #2325 (abstr.)*.

Nakashima D., Ushikubo T., Joswiak D. J., Brownlee D. E., Matrajt G., Weisberg M. K., Zolensky M. E. and Kita N. T. (2012) Oxygen isotopes in crystalline silicates of comet Wild 2: a comparison of oxygen isotope systematics between Wild 2 particles and chondritic materials. *Earth Planet. Sci. Lett.* **357–358**, 355–365.

Nguyen A. N., Stadermann F. J., Zinner E., Stroud R. M., Alexander C. M. O'D. and Nittler L. R. (2007) Characterization of presolar silicate and oxide grains in primitive carbonaceous chondrites. *Astrophys. J.* **656**, 1223–1240.

Nguyen A. N., Nittler L. R., Stadermann F. J., Stroud R. M. and Alexander C. M. O'D. (2010) Coordinated analyses of presolar grains in the Allan Hills 77307 and Queen Elizabeth Range 99177 meteorites. *Astrophys. J.* **719**, 166–189.

Nittler L. R., Alexander C. M. O'D., Davidson J., Riebe M. E. I., Stroud R. M. and Wang J. (2018) High abundances of presolar grains and ^{15}N-rich organic matter in CO3.0 chondrite Dominion Range 08006. *Geochim. Cosmochim. Acta* **226**, 107–131.

Nittler L. R., Stroud R. M., Trigo-Rodríguez J. M., De Gregorio B. T., Alexander C. M. O'D., Davidson J., Moyano-Cambero C. E. and Tanbakouei S. (2019) A cometary building block in a primitive asteroidal meteorite. *Nat. Astron* **3**, 659–666.

Raghavan V. (2004) Fe–Ni–S (iron–nickel–sulfur). *J. Phase Equilib.* **25**, 373–381.

Roth A. S. G. and Leya I. (2018) No cosmic-ray precompaction exposure of chondrules in CR2.7 MIL 090657. *Meteorit. Planet. Sci.* **53**, 2644–2651.

Rubin A. E. (2012) Collisional facilitation of aqueous alteration of CM and CV carbonaceous chondrites. *Geochim. Cosmochim. Acta* **214**, 181–194.

Satterwhite C. and Mittlefehldt D. (2001). *Antarctic Meteorite Newsletter* **24**(2).

Satterwhite C. and Righter K. (2012). *Antarctic Meteorite Newsletter* **35**(2).

Schrader D. L. and Davidson J. (2017) CM and CO chondrites: a common parent body or asteroidal neighbors? Insights from chondrule silicates. *Geochim. Cosmochim. Acta* **214**, 157–171.

Schrader D. L., Connolly, Jr., H. C. and Lauretta D. S. (2008) Opaque phases in type-II chondrules from CR2 chondrites: Implications for CR parent body formation. *Geochim. Cosmochim. Acta* **72**, 6124–6140.

Schrader D. L., Franchi I. A., Connolly, Jr., H. C., Greenwood R. C., Lauretta D. S. and Gibson J. M. (2011) The formation and alteration of the Renazzo-like carbonaceous chondrites I: implications of bulk-oxygen isotopic composition. *Geochim. Cosmochim. Acta* **75**, 308–325.

Schrader D. L., Connolly, Jr., H. C., Lauretta D. S., Nagashima K., Huss G. R., Davidson J. and Domanik K. J. (2013) The

formation and alteration of the Renazzo-like carbonaceous chondrites II: linking O-isotope composition and oxidation state of chondrule olivine. *Geochim. Cosmochim. Acta* **101**, 302–327.

Schrader D. L., Davidson J., Greenwood R. C., Franchi I. A. and Gibson J. M. (2014) A water-ice rich minor body from the early Solar System: the CR chondrite parent asteroid. *Earth Planet. Sci. Lett.* **407**, 48–60.

Schrader D. L., Connolly, Jr., H. C., Lauretta D. S., Zega T. J., Davidson J. and Domanik K. J. (2015) The formation and alteration of the Renazzo-like carbonaceous chondrites III: towards understanding the genesis of ferromagnesian chondrules. *Meteorit. Planet. Sci.* **50**, 15–50.

Schrader D. L., Nagashima K., Krot A. N., Ogliore R. C., Yin Q.-Z., Amelin Y. A., Stirling C. H. and Kaltenbach A. (2017) Distribution of ^{26}Al in the CR chondrite chondrule-forming region of the protoplanetary disk. *Geochim. Cosmochim. Acta* **201**, 275–302.

Schrader D. L., Nagashima K., Waitukaitis S. R., Davidson J., McCoy T. J., Connolly, Jr., H. C. and Lauretta D. S. (2018a) The retention of dust in protoplanetary disks: evidence from agglomeratic olivine chondrules from the outer Solar System. *Geochim. Cosmochim. Acta* **223**, 405–421.

Schrader D. L., Fu R. R., Desch S. J. and Davidson J. (2018b) The background temperature of the protoplanetary disk within the first four million years of the Solar System. *Earth Planet. Sci. Lett.* **504**, 30–37.

Scott E. R. D., Keil K. and Stöffler D. (1992) Shock metamorphism of carbonaceous chondrites. *Geochim. Cosmochim. Acta* **56**, 4281–4293.

Shewman R. W. and Clark L. A. (1970) Pentlandite Phase Relations in the Fe-Ni-S System and Notes on the Monosulfide Solid Solution. *Canad. J. Earth Sci.* **7**, 67–85.

Tenner T. J., Ushikubo T., Nakashima D., Kita N. T., Weisberg M. K. and Kimura M. (2014) Silica excess in anorthitic plagioclase from type 3.00 chondrite chondrules: Evidence for retaining primary ^{26}Al-^{26}Mg systematics. *Lunar Planet. Sci. XLV. Lunar Planet. Inst., Houston. #1187(abstr.)*.

Tenner T. J., Nakashima D., Ushikubo T., Kita N. T. and Weisberg M. K. (2015) Oxygen isotope ratios of FeO-poor chondrules in CR3 chondrites: Influence of dust enrichment and H_2O during chondrule formation. *Geochim. Cosmochim. Acta* **148**, 228–250.

Tenner T. J. (2017) Evaluating silica excess in Dominion Range 08006 chondrule plagioclase: comparisons to Yamato 81020 and Acfer 094 chondrule plagioclase. *80th Annual Meeting of the Meteoritical Society, #6394 (abstr.)*.

Van Kooten E. M. M. E., Wielandt D., Schiller M., Nagashima K., Thomen A., Larsen K. K., Olsen M. B., Nordlund K., Krot A. N. and Bizzarro M. (2016) Isotopic evidence for primordial molecular cloud material in metal-rich carbonaceous chondrites. *Proc. Natl. Acad. Sci.* **113**, 2011–2016.

Vollmer C., Hoppe P., Stadermann F. J., Floss C. and Brenker F. E. (2009) NanoSIMS analysis and Auger electron microscopy of silicate and oxide stardust from the carbonaceous chondrite Acfer 094. *Geochim. Cosmochim. Acta* **73**, 7127–7149.

Warren P. H. (2011) Stable-isotopic anomalies and the accretionary assemblage of the Earth and Mars: a subordinate role for carbonaceous chondrites. *Earth Planet. Sci. Lett.* **311**, 93–100.

Weisberg M. K., Prinz M., Clayton R. N. and Mayeda T. K. (1993) The CR (Renazzo-like) carbonaceous chondrite group and its implications. *Geochim. Cosmochim. Acta* **57**, 1567–1586.

Weisberg M. K., McCoy T. J. and Krot A. N. (2006) Systematic and evaluation of meteorite classification. In *Meteorites and the Early Solar System II* (eds. D. S. Lauretta and H. Y. McSween). University of Arizona Press, Tucson, pp. 19–52.

Wlotzka F. (2005) Cr spinel and chromite as petrogenetic indicators in ordinary chondrites: equilibration temperatures of petrologic types 3.7 to 6. *Meteorit. Planet. Sci.* **40**, 1673–1702.

Zhao X., Floss C., Stadermann F. J., Bose M. and Lin Y. (2011) Continued investigation of presolar silicate grains in the carbonaceous chondrite Ningqiang. *Lunar Planet. Sci. XLII. #1982 (abstr.)*.

Zhao X., Floss C., Lin Y. and Bose M. (2013) Stardust investigation into the CR chondrite Grove Mountain 021710. *Astrophys. J.* **769**, 49–64.

Associate editor: Sara S. Russell